Optics Letters

Multi-millijoule, few-cycle 5 µm OPCPA at 1 kHz repetition rate

Lorenz von Grafenstein,[1] **Martin Bock,**[1] **Dennis Ueberschaer,**[1]
Esmerando Escoto,[1] **Azize Koç,**[1] **Kevin Zawilski,**[2] **Peter Schunemann,**[2]
Uwe Griebner,[1,*] **and Thomas Elsaesser**[1]

[1]*Max Born Institute for Nonlinear Optics and Short Pulse Spectroscopy, Max-Born-Str. 2a, D-12489 Berlin, Germany*
[2]*BAE Systems, MER15-1813, P.O. Box 868, Nashua, New Hampshire 03061, USA*
Corresponding author: griebner@mbi-berlin.de

A table-top midwave-infrared optical parametric chirped
pulse amplification (OPCPA) system generates few-cycle
pulses with multi-10 GW peak power at a 1 kHz repetition
rate. The all-optically synchronized system utilizes $ZnGeP_2$
nonlinear crystals and a highly stable 2 µm picosecond
pump laser based on $Ho:YLiF_4$. An excellent energy extrac-
tion is achieved by reusing the pump pulse after the third
parametric power amplification stage, resulting in 3.4 mJ
idler pulses at a center wavelength of 4.9 µm. Pulses as
short as 89.4 fs are achieved, close to only five optical
cycles. Taking into account the pulse energy, a record high peak
power of 33 GW for high-energy mid-IR OPCPAs beyond
4 µm wavelength is demonstrated.

https://doi.org/10.1364/OL.402562

Today's interest in high-energy ultrafast light sources in the
mid-infrared [mid-wave infrared (MWIR) and long-wave
infrared (LWIR)] is mainly driven by the numerous applica-
tions in strong-field laser-matter interactions and attosecond
science [1,2]. The key for generating higher cutoff energies in
high harmonic generation [3] and more efficient ultrafast hard
x-ray sources [4] is the scaling law of the electrons pondero-
motive energy with the square of the laser wavelength [5,6].
For such applications, the wavelength scaling of the required
few-cycle pulses must go along with a high pulse energy, i.e., in
the millijoule (mJ) range, and kHz repetition rates to implement
sufficient detection sensitivity and signal-to-noise ratio. In addi-
tion, such sources hold strong potential for two-dimensional
(2D) infrared spectroscopy, time-resolved imaging of molecular
structures, and the implementation of novel x-ray sources [7,8].

To date, the most common technique to generate high
peak power few-cycle pulses in the mid-IR relies on optical
parametric amplifiers (OPAs) or optical parametric chirped

pulse amplifiers (OPCPAs) [9]. The majority of such high-
performance sources were realized in the spectral range below
4 µm. These systems typically utilize commercially avail-
able 1 µm pump sources and oxide crystals, like $LiNbO_3$ or
$KTiOAsO_4$ as nonlinear mediums [10–14]. Applying 1 µm
pump sources for the extension of the pulse center wavelength
beyond 4 µm, faces considerable challenges due to a lack of
suitable nonlinear crystals [15].

With the recent development of high-energy, ultrashort
pulse laser systems in the 2 µm spectral range based on holium
(Ho)-doped gain media [16–18] new roadmaps toward the
realization of mJ-level, MWIR and LWIR OPCPAs have been
established. With such pump lasers, non-oxide crystals like
$ZnGeP_2$ (ZGP, transparency range: 2–8 µm) can be applied in
high-energy, broadband parametric amplifiers, owing to their
large second-order nonlinearity ($d_{eff} > 60$ pm/V [19]), moder-
ate damage threshold, and availability with large aperture. The
bandgap energy of ZGP is about twice the 1 µm photon energy
and thus demands pump sources emitting beyond 2 µm in order
to circumvent two-photon absorption [15,19]. The recently
developed $CdSiP_2$ belongs to the same class of crystals with an
extended transparency down to 1 µm, but requires pump wave-
lengths >1.3 µm to enable broadband phase-matching. Even
though 2 µm picosecond pump lasers with energies of up to
200 mJ have been demonstrated [17], the reported pulse ener-
gies, generated beyond 4 µm via parametric down conversion,
are only slowly approaching the mJ-level.

ZGP-based OPA/OPCPAs pumped with Ho-doped regen-
erative amplifiers have generated idler pulses around 5 µm at a
1 kHz repetition rate with durations of 99 fs [16] and 105 fs [20]
and energies of 40 µJ [16] and 60 µJ [20], respectively. Using a
$Ho:YLiF_4$ (Ho:YLF) chirped pulse amplifier (CPA) as pump up
to 1000 µJ with 80 fs pulses centered at 5.0 µm were generated
at 1 kHz [21,22]. Pulses at a central wavelength of 7 µm with
700 µJ energy and 180 fs were demonstrated as well [17]. The
latter system incorporates a cryo-cooled Ho:YLF CPA as pump,
which operates at an order of magnitude lower repetition rate of
100 Hz, compared to the other referenced systems. Exploring
the coherent synthesis of signal and idler pulses in CSP by using

a 2-µm carrier-envelope-phase-stabilized OPCPA at 1 kHz as pump, 33 µJ pulses as short as 13 fs centered at 4.2 µm were achieved [23].

Here, we present, to the best of our knowledge, the first multi-mJ few-cycle OPCPA operating at a 1 kHz repetition rates in the MWIR. Pumped by a highly stable picosecond Ho:YLF CPA, the OPCPA provides idler pulses at 4.9 µm with an ultrashort pulse duration of 89.4 fs and an energy of 3.4 mJ. The compressed pulses are characterized by third-harmonic interferometric frequency-resolved optical gating (TH-iFROG).

Figure 1 shows the schematic layout of the MWIR-OPCPA. The signal and pump seed pulses for the parametric amplification are provided by a fiber-based 40 MHz multi-color laser system (Toptica). It contains three separate erbium (Er)-doped fiber amplifiers which are fed by an 80 fs Er:fiber oscillator and generates pulses at 1.55 µm as well as two supercontinua (SC). The pulses of the latter are generated separately in two highly nonlinear fibers, optimized for SC generation with their center of gravity at 1.0 and 2.0 µm, respectively. The signal pulses at 3.5 µm are provided by means of difference frequency generation of the 1.5 µm oscillator and the 1.0 µm SC-pulses. The pulses with center of gravity at 2.0 µm serve as seed for the pump channel. The latter is based on a Ho:YLF CPA operating at 2050 nm and a 1 kHz repetition rate [18]. To safely avoid crystal damage in the OPCPA, we use pump pulses of 5 ps duration and 36 mJ energy, corresponding to a peak power of 7 GW. The pulse-to-pulse stability in the 1 kHz pulse train has an excellent value below 0.3% rms and the beam quality is characterized to be better than a M-square value of 1.2.

The signal pulses, centered at 3.5 µm with a duration of 30 fs and 30 pJ pulse energy, are phase shaped in a spatial light modulator (SLM). The MWIR-SLM (Meadowlark) designed for the wavelength range from 2.8 to 4.0 µm, works in reflection, and is based on the liquid crystal silicon technology. The liquid crystal (LC) material is arranged in an array of cells with 512×512 pixels and a 25 µm pixel pitch. Despite we are eventually focusing on the idler pulses, we apply the SLM for phase-only modulation of the signal pulses, i.e., in the spectral range 3.1–3.9 µm. Compared to the idler pulses at 5 µm, a larger phase stroke is

Fig. 1. Setup of the 2 µm pumped midwave-IR OPCPA. The main parts are the all-fiber based three color front-end (f_{rep} = 40 MHz), the difference frequency generation (DFG), the 2 µm Ho:YLF chirped pulse amplifier (CPA) (f_{rep} = 1 kHz), the four optical parametric amplifier (OPA) stages based on ZGP crystals, and the phase shaper in a 4-f configuration with the reflective spatial light modulator (SLM) placed in its Fourier plane. Booster, power amplifier; DM, dichroic mirror; RA, regenerative amplifier; S, bulk stretcher; SC, supercontinuum; TFP, thin-film polarizer; Tm:fiber, pre-amplifier.

feasible and, due to the sign inversion of the chirp between the signal and idler during parametric amplification, the dispersion of the idler pulses is indirectly managed for optimal compression [22]. The shaper is constructed in a typical 4-f configuration (Fig. 1). An optical grating with 600 l/mm is used as the dispersive element, resulting in a resolution of 10 nm for independent spectral shaping. The throughput of the shaper setup is 25% with the contributing reflectivity of the SLM being 66%. The calibration procedure of our MWIR-SLM has been reported in [22] resulting in a maximum phase-shaping range for our signal spectrum of ~100 rad.

With respect to the chirp inversion between signal and idler pulses in the parametric amplification process, we use bulk materials for temporal stretching and compression in our system. In contrast to the commonly required grating arrangements in the visible and near IR spectra, a quasi-lossless management of the main contribution of the dispersion in the OPCPA, i.e., the group delay dispersion (GDD), is enabled. This sign inversion for the GDD is not present for uneven orders of the dispersion, in particular for the third (TOD). Thus, these dispersion contributions have to be managed by the SLM.

The parametric amplifier is configured in a four-stage arrangement. All stages contain ZGP crystals. Three stages, the first (OPA 1), second (OPA 2), and fourth (OPA 4), are designed in a non-collinear geometry (type-I, non-collinear angle: 2.0°, $\theta = 59°$), whereby the signal at 3.5 µm is the seed in OPA 1 and OPA 2. Only the third stage (OPA 3), also seeded with the signal pulse, is in collinear geometry (type-I, $\theta = 55°$). The latter is necessary to generate an idler pulse without angular dispersion. OPA 4 is seeded with the idler pulse generated in OPA 3 and pumped using the residual 2 µm pulse behind OPA 3. The pump intensity is 12 GW/cm² in all OPA stages. In order to ensure optimal amplification and bandwidth of the signal pulses in the OPCPA, the ratio between pump and seed pulse duration has to be adapted for each OPA stage individually by introducing bulk materials between the stages (Fig. 1). In front of OPA 1, consisting of a 3 mm thick ZGP crystal, the signal pulse is stretched to ~700 fs (FWHM) in 50 mm CaF₂. A large amount of negative TOD is imprinted on the seed pulses by the SLM, resulting in a modulated temporal envelope that covers a 2 ps time interval {cf. Fig. 3(a) in [21]}.

The amplification in OPA 1 delivers 5 µJ pulse energy (pump: 0.4 mJ). After a further stretching to 2 ps in 25 mm sapphire, the signal pulses are amplified in OPA 2 (2 mm thick ZGP crystal) to 260 µJ using 3 mJ pump energy. The signal spectra after the non-collinear stages OPA 1 and OPA 2 are similar to the ones presented in [22]. Before entering OPA 3, the collinear stage, the signal pulse passes once again a 25 mm sapphire crystal, which leads to a pulse duration of 3 ps. The main part of the 2 µm pump energy, 26 mJ, is fed into OPA 3. Because of the rather low damage threshold of ZGP (~10 GW/cm² estimated for the 5 ps pump pulses [24]), the pump beam is expanded to about 10 mm diameter and a large aperture ZGP crystal with a diameter of ~15 mm (thickness: 1.0 mm) is implemented in OPA 3. An energy of 3.5 mJ per pulse is generated in the 3.5 µm signal pulse train. The signal spectrum is shown in Fig. 2(c) (red curve) displaying a bandwidth of ~500 nm which supports a duration of sub-50 fs. The energy of the idler pulse amounts to 2.4 mJ which serves as a seed for OPA 4. The transmitted pump after OPA 3, with an energy of about 20 mJ, enters OPA 4 after loosely focusing to an 8 mm beam diameter, taking into account
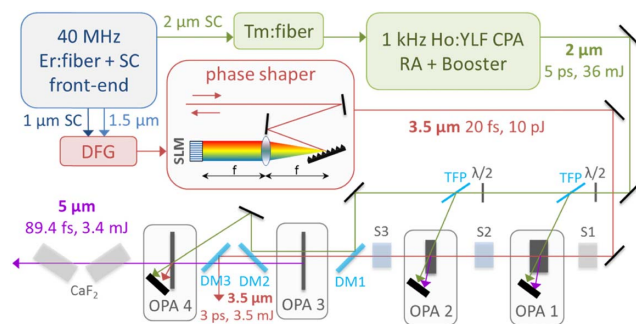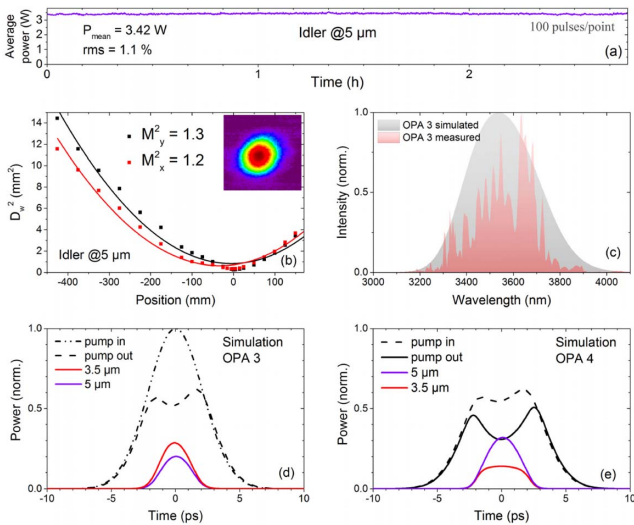
Fig. 2. OPCPA output performance characterization. (a) Long-term pulse stability of the idler; (b) beam profile of the idler (D_w–beam diameter at $1/e^2$); (c) signal spectrum after OPA 3, measured and simulated; (d), (e) simulation of the temporal pulse evolution of signal and idler in OPA 3 and OPA 4.

Fig. 3. TH-iFROG characterization of the compressed 4.9 µm pulses at a 3 mJ energy level. (a) Measured TH-iFROG trace; (b) Fourier-filtered (measured) and retrieved DC-TH-iFROG sub-traces; (c) measured (blue) and retrieved (red) collinear ACF; (d) measured (gray) and retrieved (brown) optical spectrum and phase (blue). (e) FTL (gray) and retrieved temporal pulse shape (brown) and phase (blue).

the nonlinear refractive index contribution of ZGP in OPA 3. In the 0.8 mm thick ZGP crystal, the idler pulse energy is amplified to its final value of 3.4 mJ in the 1 kHz pulse train. The measured excellent long-term pulse stability with a power fluctuation rms of 1.1% and the nearly diffraction-limited beam profile with an $M^2 \le 1.3$ of the idler (error: 13%) are shown in Figs. 2(a) and 2(b), respectively. The error is related to the uncertainty of the measurement in the focal area due to the large pixel size (80 µm) of the camera (Pyrocam, Ophir).

Because the residual 2 µm beam after OPA 3 is used to pump OPA 4, pump depletion and parametric gain have to be carefully balanced between OPA 3 and OPA 4. For estimation of the pump depletion, the signal spectrum is simulated assuming a Gaussian-shaped seed spectrum [Fig. 2(c), gray curve]. Using the Sisyfos code [25], Fig. 2(d) shows a simulation of the temporal pulse evolution in OPA 3 with a pump intensity of $12 \, GW/cm^2$ and a signal intensity of $133 \, MW/cm^2$ in the 1.0 mm thick ZGP crystal. Figure 2(e) displays the outcome of the corresponding simulation in OPA 4 with altered pump and idler pulses from OPA 3 in the 0.8 mm thick ZGP of OPA 4. In OPA 3, a conversion efficiency from pump to idler of about 10% is expected, further boosted to 14% with OPA 4. These values fit our experimental values of 9.6% and 13.6% quite well. Superfluorescence contributes 2% to the total output power after OPA 3, as measured by blocking the signal seed pulse. A similar measurement after OPA 4 was not feasible because of potential crystal damage by the undepleted pump pulse.

The idler spectrum extends from 4.5 to 5.4 µm (at $1/e^2$) which supports a Fourier transform limited (FTL) pulse duration of 60 fs [Fig. 3(d)]. The structuring of the idler spectrum is attributed to various factors. The LC absorption of the SLM is manifested in the dip at 5.2 µm. The strong CO_2 absorption band at 4.25 µm limits the idler spectrum on the short wavelength side [along with the edge of dichroic mirror (DM)1], while above 5.2 µm the absorption lines of water vapor in the atmosphere structure the spectrum. Such limitations can be overcome by purging the system with, e.g., nitrogen. We
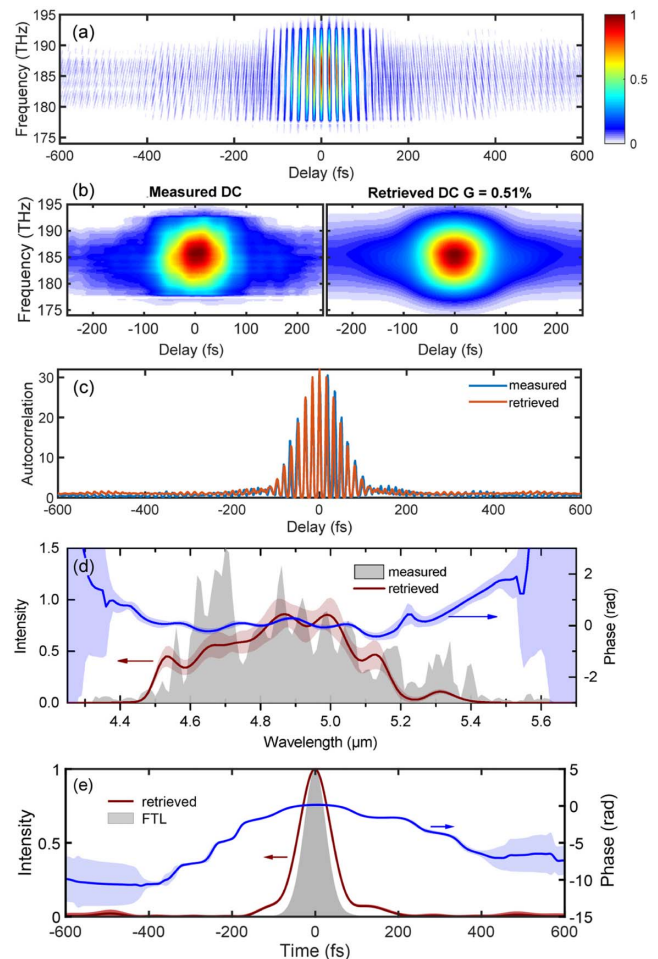
attribute the high-frequency modulation, which extends over the entire spectrum, to the pixel array structure of the SLM and the strong temporal modulation of the signal pulses by the imprinted TOD.

Re-compression of the idler pulses was achieved by propagation through four 25 mm long CaF_2 crystals placed at Brewster's angle. The TOD amounting to $9 \times 10^5 \, fs^3$ and higher order dispersion as well as the remaining GDD of the pulses is managed by phase shaping at the SLM. The idler pulses are characterized by applying TH-iFROG [26]. $AgGeS_2$ crystals are used to generate the second harmonic (SH) and subsequently the TH by sum-frequency generation, both in a collinear geometry.

Figures 3(a)–3(e) show the measured and retrieved TH-iFROG traces. TH-iFROG includes THG-FROG traces as a limiting case, uniquely retrieves the pulse shape, and provides accuracy checks and corrections [26]. In addition, TH-iFROG allows the correction of delay jitters and provides access to three unique sub-traces, direct-current (DC), fundamental modulation (FM) and SH modulation (SHM). All sub-traces are extracted via Fourier-filtering and are analyzed simultaneously

by one retrieval algorithm, through the differential evolution method. Starting from the raw interferometric TH-iFROG trace [Fig. 3(a)], marginal correction [26] is performed using an independently-measured fundamental spectrum, after the subtraction of noise-like artifacts. Each FROG sub-trace can be used individually to retrieve the pulse. We include all three sub-traces for retrieval, but assign different weights to each, representing how much their reconstruction error affects the total error. The DC sub-trace is assigned a weight of 1, the FM sub-trace a weight of 0.5, and the SHM sub-trace 0.25. The weights are based on the quality of the extracted sub-traces. Out of the three extracted sub-traces the DC one is presented in Fig. 3(b) displaying the measured and the retrieved DC-TH-iFROG sub-traces, respectively. The so-called FROG error G, qualifying the difference of the measured and retrieved traces is 0.51% for the DC sub-trace, which is a good value given the artifacts in the trace (grid size of the trace: 1201×370). Aside from the low retrieval error, the accuracy of the retrieval is also corroborated by the collinear autocorrelation function (ACF) of our pulse which is presented in Fig. 3(c) together with the measured ACF. The spectrum of the idler is also well reconstructed [Fig. 3(d)] even if the frequency of the slight modulations differs between measured and retrieved spectrum. The latter is attributed to the different spectral resolutions of the spectrometer devices used for measuring the idler (Horiba monochromator: 0.1 nm) and the TH spectrum (Ocean Optics, NIRQuest: 3 nm). The retrieved pulse characteristics in the time-domain delivered a pulse duration as short as 89.4 fs [Fig. 3(e), brown curve]. Further reduction of the pulse width to the FTL duration of 60 fs is hampered by the strong phase modulation due to pulse propagation in air. The very weak satellite structures at -500 fs and $+500$ fs are attributed to the already discussed diffraction related to the pixel array structure of the SLM and contain less than 5% of the pulse energy. A scan of the full pump pulse amplification window confirmed that no other pre- or post-pulses are detectable.

The 89.4 fs pulse duration centered at 4.9 µm is close to only five optical cycles. Taking into account the energy content of the satellites, the idler pulse energy of 3.4 mJ translates into a record peak power of 33 GW.

In conclusion, we have demonstrated a 5 µm OPCPA system delivering multi-10 GW femtosecond pulses at a 1 kHz repetition rate. Pumped at 2.05 µm, idler pulses with up to 3.4 mJ energy were generated in the 1 kHz pulse train representing the highest to date of any fs mid-IR source beyond 4 µm. The dispersion management in the ZGP-based OPCPA with bulk material in combination with phase shaping of the signal allows for a flexible adaptation to the residual spectral phase for the idler. The latter leads to an idler pulse duration as short as 89.4 fs. These pulse characteristics represent the highest peak power of 33 GW achieved for MWIR OPCPAs to the best of our knowledge, and, if focused to a 15 µm spot diameter, would reach a peak intensity of $>10^{16}$ W/cm^2. The system appears scalable with respect to higher pulse peak power by purging the parametric amplifier chain to get access to the full generated optical spectrum and, thus, to potentially shorter re-compressed pulses.

REFERENCES

1. B. Wolter, M. G. Pullen, M. Baudisch, M. Sclafani, M. Hemmer, A. Senftleben, C. D. Schröter, J. Ullrich, R. Moshammer, and J. Biegert, Phys. Rev. X **5**, 021034 (2015).
2. F. Krausz and M. Ivanov, Rev. Mod. Phys. **81**, 163 (2009).
3. T. Popmintchev, M.-C. Chen, D. Popmintchev, P. Arpin, S. Brown, S. Ališauskas, G. Andriukaitis, T. Balčiunas, O. D. Mücke, A. Pugzlys, A. Baltuška, B. Shim, S. E. Schrauth, A. Gaeta, C. Hernández-García, L. Plaja, A. Becker, A. Jaron-Becker, M. M. Murnane, and H. C. Kapteyn, Science **336**, 1287 (2012).
4. J. Weisshaupt, V. Juvé, M. Holtz, M. Woerner, and T. Elsaesser, Struct. Dyn. **2**, 024102 (2015).
5. P. B. Corkum, Phys. Rev. Lett. **71**, 1994 (1993).
6. J. L. Krause, K. J. Schafer, and K. C. Kulander, Phys. Rev. Lett. **68**, 3535 (1992).
7. C. Calabrese, A. M. Stingel, L. Shen, and P. B. Petersen, Opt. Lett. **37**, 2265 (2012).
8. J. Weisshaupt, V. Juvé, M. Holtz, S. A. Ku, M. Woerner, T. Elsaesser, S. Ališauskas, A. Pugžlys, and A. Baltuška, Nat. Photonics **8**, 927 (2014).
9. A. G. Ciriolo, M. Negro, M. Devetta, E. Cinquanta, D. Faccialà, A. Pusala, S. De Silvestri, S. Stagira, and C. Vozzi, Appl. Sci. **7**, 265 (2017).
10. G. Andriukaitis, T. Balčiunas, S. Ališauskas, A. Pugžlys, A. Baltuška, T. Popmintchev, M.-C. Chen, M. M. Murnane, and H. C. Kapteyn, Opt. Lett. **36**, 2755 (2011).
11. M. Baudisch, H. Pires, H. Ishizuki, T. Taira, M. Hemmer, and J. Biegert, J. Opt. **17**, 094002 (2015).
12. M. Mero, Z. Heiner, V. Petrov, H. Rottke, F. Branchi, G. M. Thomas, and M. J. J. Vrakking, Opt. Lett. **43**, 5246 (2018).
13. N. Thiré, R. Maksimenka, B. Kiss, C. Ferchaud, P. Bizouard, E. Cormier, K. Osvay, and N. Forget, Opt. Express **25**, 1505 (2017).
14. J. Pupeikis, P.-A. Chevreuil, N. Bigler, L. Gallmann, C. R. Phillips, and U. Keller, Optica **7**, 168 (2020).
15. V. Petrov, Prog. Quantum Electron. **42**, 1 (2015).
16. P. Malevich, T. Kanai, H. Hoogland, R. Holzwarth, A. Baltuška, and A. Pugžlys, Opt. Lett. **41**, 930 (2016).
17. U. Elu, T. Steinle, D. Sánchez, L. Maidment, K. Zawilski, P. Schunemann, U. Zeitner, C. Simon-Boisson, and J. Biegert, Opt. Lett. **44**, 3194 (2019).
18. L. von Grafenstein, M. Bock, D. Ueberschaer, A. Koc, U. Griebner, and T. Elsaesser, Opt. Lett. **45**, 3836 (2020).
19. P. G. Schunemann, K. T. Zawilski, L. A. Pomeranz, D. J. Creeden, and P. A. Budni, J. Opt. Soc. Am. B **33**, D36 (2016).
20. S. Cheng, G. Chatterjee, F. Tellkamp, T. Lang, A. Ruehl, I. Hartl, and R. J. D. Miller, Opt. Lett. **45**, 2255 (2020).
21. L. von Grafenstein, M. Bock, D. Ueberschaer, K. Zawilski, P. Schunemann, U. Griebner, and T. Elsaesser, Opt. Lett. **42**, 3796 (2017).
22. M. Bock, L. von Grafenstein, U. Griebner, and T. Elsaesser, J. Opt. Soc. Am. B **35**, C18 (2018).
23. H. Liang, P. Krogen, Z. Wang, H. Park, T. Kroh, K. Zawilski, P. Schunemann, J. Moses, L. F. DiMauro, F. X. Kärtner, and K.-H. Hong, Nat. Commun. **8**, 141 (2017).
24. U. Griebner, L. von Grafenstein, M. Bock, and T. Elsaesser, Proc. SPIE **10713**, 107130W (2018).
25. G. Arisholm, J. Opt. Soc. Am. B **14**, 2543 (1997).
26. J. Hyyti, E. Escoto, and G. Steinmeyer, J. Opt. Soc. Am. B **34**, 2367 (2017).